Periodic Forcing of the Swift-Hohenberg Equation in Time

Punit Gandhi,* Cédric Beaume, and Edgar Knobloch

Department of Physics, University of California, Berkeley CA 94720, USA

(Dated: May 25, 2014)

Abstract

(NEED TO WRITE A REAL ABSTRACT.) Systems with a periodic forcing in time abound! We use the generalized Swift-Hohenberg equation with a quadratic-cubic nonlinearity as test-bed for studying localized pattern formation in such systems with a periodic forcing in time. A sinisiodal linear forcing is applied to the SHE in order to the examine the dependence of localization on the amplitude, oscillation period, and offset of the time-periodic forcing. As one might expect, the region of existence of localized solutions dramatically decreases as the system is "jiggled." The parameter space within the pinning region of the constant forcing case, however, is partitioned into regions of growth, stability, and decay with an unexpected structure when large oscillations are applied.

* punit_gandhi@berkeley.edu

I. INTRODUCTION

Time-dependent forcing can be critical to the understanding of pattern formation in certain systems. Daily and seasonal variations of insolar flux due to the Earth's rotation and orbit, for example, provide a periodic forcing for many ecological systems [1–5]. Furthermore,periodic and stochastic switching between systems in time have been shown to produce new "ghost" attractors that do not exist in either time-independent systems or the averaged system. Studies have observed this phenomon in coupled oscillator systems[6] and have used it to create patterned states from systems where they would not otherwise exist [7]. Even systems that are designed to have a constant forcing may have a time-dependence introduced by noise or other experimental considerations. This unintentional time dependence could destabilize certain states, making them impossible to achieve experimentally. This is particularly true of spacially localized patterns that often exist within a narrow region of parameter space. oscillations in time could also have the opposite effect of stabilizing a previously unstable stationary solution. Indeed, the inverted pendulum attached to a vertically oscillating base provides an example of this- the upright position of the pendulum can be stabilized if the oscillations are fast enough.

The Swift–Hohenberg equation [8] (SHE) serves as a model for pattern formation in a broad range of physical systems. The existence, structure, and stability of localized solutions within the SHE has been studied in great detail [9–11]. This equation which, in one dimension, takes the form

$$u_t = ru - \left(1 + \partial_x^2\right)^2 u + N[u], \tag{1}$$

describes the dynamics of a real field u over one spatial dimension in time, where N is some nonlinear function of u. We have rescaled the equation so that the characteristic wavenumber that defines the natural wavelength of the patterned state is unity. Two possible choices of N, namely $N_{23}[u] = bu^2 - u^3$ and $N_{35}[u] = bu^3 - u^5$, are often considered because of the different symmetries they possess. This study focuses on the more simple N_{23} that provides the equation with only one reflection symmetry for a given arbitrary axis ($x \to -x$, $u \to u$). Preliminary numerical simulations indicate, however, that analgous behaviors to the results obtained here are found in the case of N_{35} (SHOULD WE CHECK THAT THIS IS TRUE AND INCLUDE A STATEMENT LIKE THIS?) The strength of the linear forcing term r and the strength of the quadratic nonlinearity b are left as parameters of the system. In

order to study the effects of time-dependence, we will include an addtional periodic term to the linear forcing, namely $r \to r_0 + \rho \sin \omega t$, where r_0, ρ, and $\omega = 2\pi/T$ define the offset, amplitude, and frequency of the oscillation.

All simulations in time used periodic boundary conditions on a domain of $L = 80\pi$ (e.g. 40 characteristic wavelengths), unless otherwise noted. A 4th order exponential time differencing scheme[12] was used to step forward in time while spectral methods on a grid of 1024 points were used for the spatial calculations. In cases where a larger domain was necessary, the spatial density of grid points was kept constant. Steady state solutions of the constant forcing case were computed by numerical continuation using AUTO [13].

We first recount the relevant details of the Swift-Hohenberg equation with a constant forcing before discussing some numerical results and theoretical analysis of the periodically forced case. We begin by examining the effect of small oscillations on the growth and decay of slightly unstable localized solutions, and then move to large oscillations that extend through and beyond the pinning region of the constant forcing case. Finally, discuss the persistence of a localized defect state that would be unstable without the oscillations before concluding with a summary of the results and an outlook on future work.

II. PATTERNS AND SPATIAL LOCALIZATION WITH A CONSTANT FORCING

NEED HELP WITH THE WORDING HERE

In this section, we describe the structure and some relevant properties of the solutions of SHE (Eq. 8) with a constant forcing. Because SHE can be written in terms of the variation of a Lyaponov functional (we will refer to this as the "Free Energy" of the system)

$$\mathcal{F}[u] = -\frac{1}{L} \int_{-L/2}^{L/2} \tfrac{1}{2} r u^2 - \tfrac{1}{2} \left[(1+\partial_x^2)u\right]^2 + M[u]\, dx \tag{2}$$

where $\delta M/\delta u = N$, the solution will approach a steady-state in time that corresponds to a local minimum of this free energy if given appropriate boundary conditions (NEED TO MAKE THIS MORE PRECISE). If we consider the space of steady-state solutions, we find that a periodic solution u_p ($u_p(x) = u_p(x + 2\pi)$), is formed from a bifurcation at $r = 0$ where the trivial solution $u_0 = 0$ changes stability. On a finite domain, the domain size

and boundary conditions will determine a series of periodic solutions of differing period that emerge from the trivial branch for $r > 0$ as it becomes more and more unstable. We will focus on the case that the periodic branches emerge subcritically and the trivial branch becomes unstable in time for $r > 0$.

A. Structure of stationary solutions in and out of the pinning region

For a suitable choice of b, there exists a Maxwell point for a particular value of the forcing ($r = r(M)$) where the energy ($\mathcal{F}[u_p] = \mathcal{F}[u_0] = 0$) and a pinning region around it where the energy between the trivial and periodic states is sufficiently close that stable localized states formed from fronts between the two can also exist. A bifurcation diagram of the steady state solutions (Fig. 1, from J. Burke et et al NEED TO REPLACE WITH MY OWN) or Fig. 2 shows the trivial state, a periodic state, and localized solution branch within the pinning region . For our choice of parameter $b = 1.8$ and a domain size $L = 80\pi$ (e.g. 40 characteristic wavelengths), the trivial solution is stable for $r < 0$ and becomes unstable as as the periodic solution with 40 periods (P_{40}) is created through a bifurcation at $r = 0$. As we are looking at the subcritical case, we see a saddle-node bifurcation of the periodic branch where it gains stability at SN_P. Thus we have only a stable trivial solution for $r < r(SN_P) \approx -0.3744$. At this point, a stable (and unstable) periodic solution is created but is energetically unfavorable to the trivial state. For $r(E_-) < r < r(E_+)$, we have a zoo of localized solutions (including an entire sequence of stable localized solutions on each snaking branch) that exist in addition to the stable trivial and periodic solutions. We note that within this region, $r(M)$ indicates the transition from the trivial state being energetically favorable to the periodic state becoming energetically favorable. Between $r(E_+)$ and $r = 0$, we again have only the periodic solution and the trivial solution as stable but with the periodic solution now more energetically favorable. Finally, for $r > 0$, the trivial solution looses stability and only the periodic solution remains as stable. We note that other stable solutions exist (e.g. the flat, nonzero solutions created at the transcritical bifurcation at $r = 1$) but that they have not been found to play a role in our region of interest with our current choice of parameters. (NEED TO INCLUDE DEFINITIONS OF FRONT VARIABLE AND ALSO INCLUDE A GRAPH OF THE STATIONARY SOLUTIONS IN AMPLITUDE FRONT SPACE)

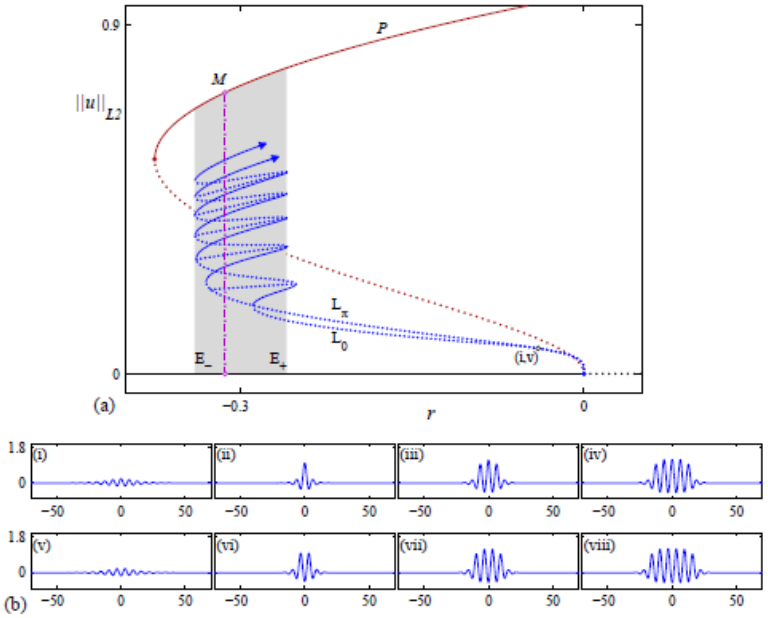

FIG. 1: This figure was taken from Burke[] (a) Bifurcation diagram showing the snakes-and-ladders structure of localized states. Away from the origin the snaking branches L_0 and L_- are contained within the snaking region (shaded) betweenE_- and E_+, where $r(E_-) \approx -0.3390$ and $r(E_+) \approx -0.2593$. Solid (dotted) lines indicate stable (unstable) states. In addition, the Maxwell point M, occurring at $r(M) \approx -0.3128$ is indicated with a vertical dash-dot line. The saddle node bifurcation that creates the stable periodic state occurs at $r < r(SN_P) \approx -0.3744$, defining the left edge of the bistability region. We will also find it useful to define the center of the snaking region C, which corresponds to the forcing parameter $r(C) \approx -0.2992$. (b) Sample localized profiles $u(x) : (i - iv)$ lie on L_0, near onset and at the 1st, 3rd, and 5th saddle-nodes from the bottom, respectively; (v-viii) lie on L_-, near onset and at the 1st, 3rd, and 5th saddle-nodes, respectively. Parameters: $b = 1.8$.

B. Depinning of localized solutions outside of the pinning region

The dynamics solutions near steady-state have also been considered. Burke and Knobloch [9] have shown that near the pinning region (e.g. for $r = r(E_\pm) \pm \delta$ where $\delta << 1$), a localized solution that was stable at the edge of the pinning region will move towards the more energetically favorable of the trivial and the periodic state at a constant rate. Above

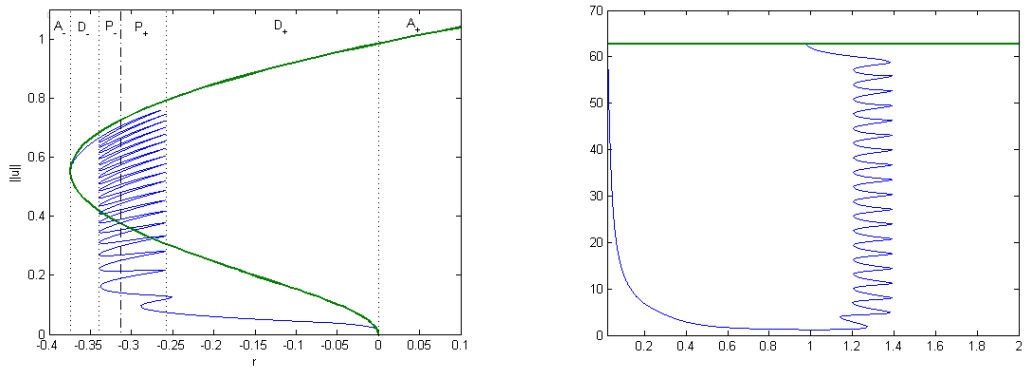

(a) (b)

FIG. 2: (a) a bifurcation diagram indicating the steady state solution structure for the various regions of interest as a fuction of the forcing r: decay by on overall amplitude dominates in A_-, period by period decay in the depinning region D_-, localized solutions are pinned in the regions $P_\pm$ near the Maxwell point (indicated with a dash-dot line), period by period nucleation occurs in the depinning region $D+$, and an overall amplitude increase towards the periodic state dominates in A_+. NEED TO CONFIRM A_+ . (b) The same steady state solutions are now plotted in phase space slice of the maximum value of the solution and the position of the front.

the snaking region, for example, a localized solution will nucleate periods of the pattern in quick bursts with some longer transition time $T_{\rm nuc} \propto \delta^{-1/2}$ in between each nucleation event.

An numerical example of this on a domain of 40 periods of the characteristic wavelength is shown in Fig. 3. A localized solution that is stable for $r = r(E_+)$ is initialized above the snaking region (e.g. $r = r(E_+)+?\delta?$) and allowed to grow until it fills the domain. We can see from Fig. 4 (NEED A BETTER FIGURE HERE) that the time from one nucleation event to the next is approximately ??, though the last nucleation event seems to take a bit longer.

We show the results of simulations for our parameters (Fig. 4) to numerically confirm the $T_{nuc} \propto \delta^{-1/2}$ law and locate the region of validity (INCLUDE LINE FROM BURKE CALCULATION ON GRAPH TO COMPARE). We also show a graph of the front speed (calculated as $2\pi/T_{nuc}$) as a function of r_0 for the constant forcing case. It is clear from these graphs, that the front moves faster to the left of pinning region in the parameter regime we

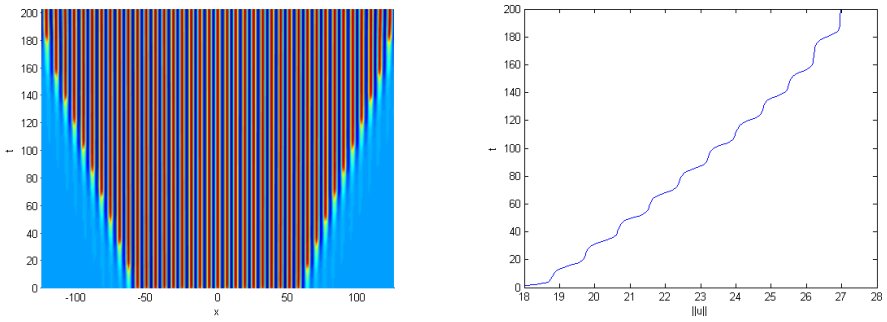

(a) (b)

FIG. 3: A simulation of the SHE with N_{23}, $b = 1.8$ and $r = -0.20$ (e.g. $\delta \approx 0.06$) is initialized using a localized solution that is stable within the snaking region (e.g. at $r = -0.2944$). The solution growing in time (a) with red as high values and blue as low values. The norm of the solution as it grows in time is shown in (b). We note that the solution fills the domain with a period solution containing 39 periods on a domain of 40 characteristic wavelengths.

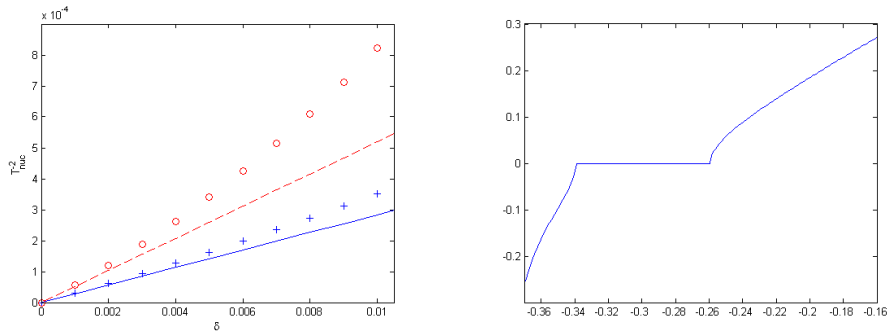

(a) (b)

FIG. 4: Simulation of the SHE with N_{23} with $b = 1.8$ show (a) $1/T_{nuc}^2$, where T_{nuc} is the time between nucleation/decay events, as a function of distance from the edge of the pinning region δ, and (b) the front speed as a function of the forcing parameter. We note that the initial solution used in these simulations was on a saddle node bifurcation of snaking branch at the closest edge of the pinning region.

are looking at. We also see a transition occur near $r = r(SN_P)$ where the solution no longer

decays period by period, but begins to decay by an overall amplitude decrease to the trivial state. Figure **??** compares the decay of a large but localized solution inititialized on a 160 period domain just above and below $r(SN_P)$. (I NEED TO REDO THESE WITH THE SOLUTION SCALED TO THE AMPLITUDE OF THE PERIODIC SOLUTION AND MAKE EPS FILES OF THEM)

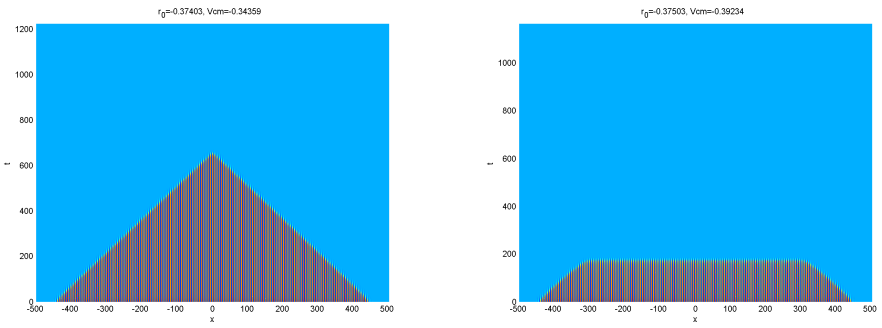

(a) (b)

FIG. 5: Decay of a localized solution that is stable at $r(E_-)$ and has been initialized with a forcing (a) above $r(SN_P)$, $r \approx -.374$ and (b) below $r(SN_P)$, $r \approx -.375$. We see a transition from decaying period by period towards the trivial solution to decaying by an overall amplitude decrease towards the trivial solution.

We also note that beyond δ of about 0.036, the decays of periods of the solutions to the left of the pinning region are no longer clearly separated by a period of slow change in the solution. Beyond this value, instead of depinning, the solution approaches the trivial stat by an overall amplitude decay.

C. Eckhaus instability and connection of snaking branch to different period periodic branch

A zoom in of the region around the bifurcation at $r = 0$ (Fig. 6a) shows the bifurcation reveals a second periodic branch with 39 periods on the domain (P_{39}) emerging from the trivial solution at a slightly positive r. The snaking branch, which forms at a secondary bifurcation on P_{40} (Fig. 6b), actually reconnects to P_{39} (Fig. 6c). Furthermore, the depinning solution shown Fig. 4 grows to a solution containing 39 periods even though the

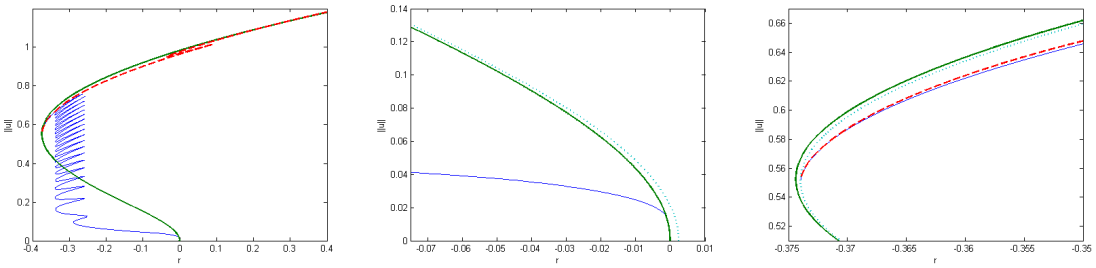

(a) (b) (c)

FIG. 6: (a) An unstable defect solution branch is shown (red dashed line) on the bifurcation diagram. (b) This defect branch emerges from the periodic branch P_{39} (light blue dotted line) where the snaking branch with a peak at the center of the localized solutions (blue solid line) reconnects. (c) P_{39} is formed from a bifurcation on the trivial branch at r slightly greater than zero.

simulation was initialized with a solution on the snaking branch that emerges from P_{40}. This phenomenon has been explained [14] in terms of the Eckhaus instability for the case of the steady state solutions. Intuitively, the wavelength of the localized solution is slightly longer than the characteristic wavelength of the solution because the more energetically favorable periodic state wants to expand into the trivial state. As the localized solution grows to a domain filling size, it finds that there isn't enough room to nucleate the 40th wavelenth of the solution. Because we are outside of the region that is Eckhaus stable, the wavelenth instead grows to fill the domain with 39 periods.

In addition, there is a branch of stationary defect solutions that extends out into the positive forcing region (Fig. 7). Theses solutions have 39 full periods, but with a wavelength between the solutions on P_{39} and P_{40}. Thus there is not enough room to fit a 40th period and the solution is not long enough to fill the domain. The branch is formed just above the saddle node of P_{39}, where the snaking branch connects(red dotted line in Fig. 6c). We show a sample solution within the pinning region and for $r > 0$ (Fig. 7b,c). NEED TO CHECK STABILITY AND, IF UNSTABLE, WHICH PERIODIC SOLUTION ATTRACTS IT. Note that solutions have been translated to put the defect in the center (we assume periodic boundary conditions), but the front position f has be calculated assuming the defect is on the edge of the domain. One final comment about these solutions is that this defect branch

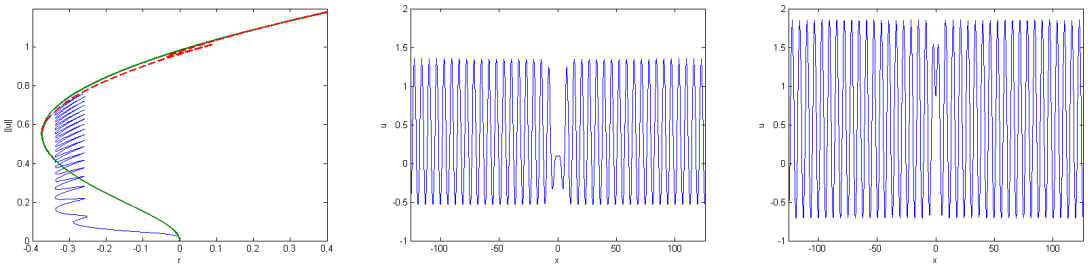

(a) (b) (c)

FIG. 7: (a) An unstable defect solution branch is shown (red dashed line) on the bifurcation diagram. A defect solution for the constant forcing case that is stationary at (b) a value of r within the pinning region and at (c) a positive value of r .

has the opposite parity of the snaking branch that emerges from P_{40} and reconnects to P_{39} in the sense that, with the defect at the edge of the domain, the center point is a minimum instead of a maximum.

D. Description of simple toy model of SHE and nucleations??

III. PERIODICALLY FORCED LOCALIZED PATTERNS

Oscillations in time arise due to imperfect control of the forcing in experiments or to fluctuating external conditions in nature. Studies of pattern formation in time-dependent systems have illustrated that non-trivial behaviors can easily be observed [15, 16]. In particular, patterns absent from steady systems can be reached when the parametric conditions are changed back and forth in a periodic way between two steady configurations. This has been shown in the Swift–Hohenberg equation, where two configurations known for exhibiting spatially homogeneous states are alterned sufficiently rapidly to give rise to oscillatory patterns [7]. In a more recent example, Belykh *et al.* [6] designed two simple systems. One of them admits one and only fixed point, attracting all initial conditions. The other system admits the same fixed point, albeit repelling, and an attracting periodic orbit. A random switch is implemented that allows to jump from one system to the other while the dynamics runs its course. When the switching is done fast enough, one expects the system to behave

like an averaged system. In their case, the averaged system is bistable between the periodic orbit and the fixed point and admits an additional unstable solution. The authors found that this unstable solution was acting as a ghost attractor in the switching system, the switch providing a stochastic law for the time spent by the solution close to the ghost.

The one-dimensional Swift–Hohenberg equation provides a more complex framework: phase space is infinite dimensional and a large number of solutions coexist. We are particularly interested in the fate of spatially localized initial conditions subject to oscillatory forcing. It is not rare that the snaking region comprising most of the spatially localized solutions be small in extent (typically less than 1% [17–19] and rarely up to 10% of the total forcing [20]). Thus, we restrict our attention to the effect of smooth oscillations bringing the system from regimes that are subcritical to some supercritical to the snaking and back again, i.e. $r(t) = r_0 + \rho\sin(\omega t)$ where $r_0 - \rho < r_l$ and $r_0 + \rho > r_r$ with r_0 the center of oscillation, ρ the amplitude of oscillation. In this case, the picture can be simplified in the following way:

- Regime 1: on the left of the snaking, below the saddle-node of the periodic branch $r < r_P$, only one stable state is observed: the trivial one.

- Regime 2: on the left of the snaking, but close enough, there is competition between two stable states: the trivial and the spatially periodic ones. In this region, the free energy of the trivial state is lower than that of the spatially periodic one ($r < r_M$). As a result, spatially localized initial conditions taken on the left of the snaking would lose rolls and decay down to the trivial solution.

- Regime 3: in the snaking region, there is a large number of coexisting states: trivial, spatially periodic and spatially localized with varied number of rolls. The interaction between all these states is complex and depends on their respective non-trivial basin of attraction.

- Regime 4: on the right of the snaking, but for $r < 0$, the same competition as on the left of the snaking arises, however, this region is above the Maxwell point. The spatially periodic state has lower energy than the trivial state and spatially localized initial conditions would nucleate rolls to eventually settle on the spatially periodic fixed point.

FIG. 8: **Write this down.**

- Regime 5: on the right of the snaking, but for $r > 0$, the only stable state relevant is the spatially periodic one.

These regimes are depicted in the phase portraits in figure 8.

The figure also introduces values that will be important to the understanding of the dynamics: $A = \max(u)$ which is the amplitude of the pattern and f =??? which is a measure of the size of the localized pattern, i.e., the distance between the pinning fronts. In addition, figure 8 displays the dominant dynamics of a spatially localized state in the given regime. When the conditions are those of regime 1, the dominant dynamics is that of a body mode and any localized initial condition sees its amplitude drop homogeneously before dying out. This regime is reached when we are far away from the snaking, but not necessarily below the saddle-node of the periodic states. There can therefore be spatially periodic solutions to complete the picture but these are not found to interact with the dynamics of spatially localized solutions. The second regime is reached closer to the snaking but still for $r < r_l$. This regime is bistable but most spatially localized structures are eventually attracted by the trivial solution. The typical decay of these solutions is dominated by an edge mode that is responsible for the progressive vanishing of the end rolls while the amplitude of the other rolls is maintained. Only once the structure is small enough in extent does the amplitude drops and the solution converges to the trivial state. The third regime corresponds to the snaking region where localized solutions are present in their time-independent form. Spatially localized initial conditions in this region tend to converge to the closest stable stationary localized snaking solution. When r is increased above the snaking region, spatially localized initial conditions transition to the spatially periodic state. For $r < 0$ (regime 4), the background trivial state is stable and the localized pattern grows by adding rolls under the influence of the edge mode until the pattern fills the domain. In regime 5, the background state is unstable and rolls start to grow everywhere, leading to a fast transition to the spatially periodic solution. Note that in figure 8, regimes 4 and 5 are undistinguishable. This does not harm the interpretation of our results as we focus on regimes 2 and 4 with excursions into regime 3 and despite often reaching regime 1 for brief

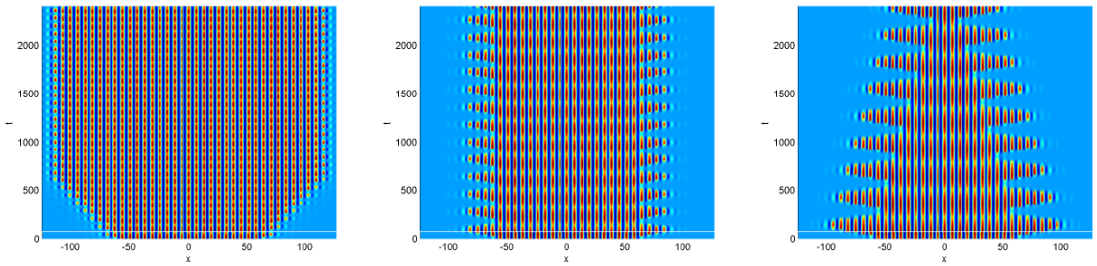

(a) $T = 80$ (b) $T = 180$ (c) $T = 280$

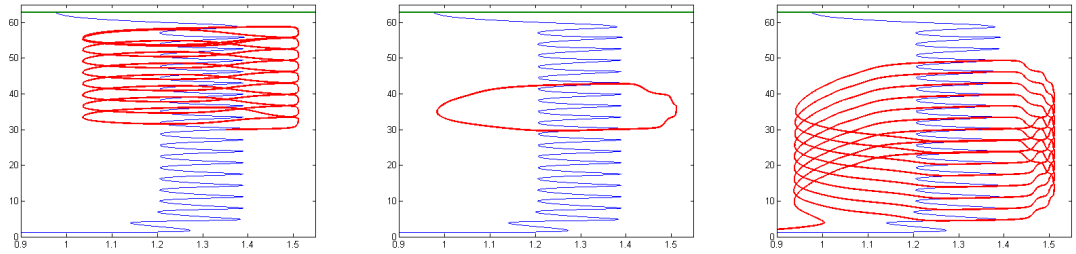

(d) $T = 80$ (e) $T = 180$ (f) $T = 280$

FIG. 9: Preliminary simulations initialized by a stationary spatially localized solution at $r = -0.28$. The forcing parameter is chosen to be $r(t) = -0.28 + 0.1\sin(2\pi t/T)$. (a)–(c) show the solution in a space-time plot; (d)–(f) represents the same phase portrait as in figure **??**. Snaking solutions and the spatially periodic branch are shown in ???. The period T is indicated below each plot.

moments, we never reached regime 5.

Figure 9 shows the outcome of preliminary simulations revealing unexpected behaviors.

The simulations have been set up using the same stationary spatially localized solution at $r = -0.28$ as initial condition and the time-dependent forcing parameter is given by $r(t) = -0.28 + 0.1\sin(2\pi t/T)$ where T is a variable period indicated in the figure. All the three simulations have been performed with identical conditions except for the forcing period. Figure 9(b,e) shows a stable periodic orbit obtained for $T = 180$, indicating that excursions in regimes 2 and 4 compensate each other by removing and nucleating 4 rolls successively. If the period is changed to a lower value ($T = 80$ in figure 9(a,d)) or a higher value ($T = 280$ in figure 9(c,f)), no periodic orbit is reached in the first place. Instead the

initial condition evolved into transients consisting of moving fronts. The former case exhibits progressive nucleation of rolls, one per period, while the latter shows progressive shrinking of the structure, with the same rate per period, until the amplitude vanishes (see phase portrait in figure **??**(e)). We investigate in the next section the existence of stable periodic orbits as the period T and the center of the oscillations r_0 are varied. Another interesting feature is shown for $T = 80$ (figures 9(a,d)), where the solution grows by nucleating one roll during each period but does not settle onto the spatially periodic state. The end state is rather a periodic orbit presenting a defect at the edge of the (periodic) domain. This ghost solution is investigated further in a later section.

A. stuff that punit thought might fit into this section from before cedric wrote it

As a proxy for the location of the front, we track the front of solution in terms of its first moment on half the domain:

$$X_{cm} = \frac{1}{||u||} \int_0^{L/2} x u^2 dx \tag{3}$$

where

$$||u|| = \int_0^{L/2} |u|^2 dx \tag{4}$$

This give half the distance from the center of the domain to the edge of a localized solution. The speed is then defined by $V_{cm} = dX_{cm}/dt$, and is really half the speed of the front.

We note that changing the phase of the oscillation in the forcing (e.g. $\rho \to -\rho$) does not seem to affect the stable region in this graph. There is a symmetry of the equation $\rho \to -\rho$, and $t \to -t$.

In an attempt to provide some context to the results in the we define the "oscillating Maxwell point" in the oscillation center r_0 where the average free energy along an oscillation of solution that is stable in time and periodic in space equals the free energy of the trivial solution (e.g. zero). For the parameter $\rho = 0.1$, we find this value to be shifted to the left by about 0.5 from the Maxwell point of the constant forcing case to $r_* \approx -0.318$ (Fig. **??**. The average free energy of oscillation does not have a strong dependence on the oscillation frequency, except that the stable oscillating solution does not exist for very slow frequencies in some cases. This is because the oscillations take the system well beyond the saddle-node

where the stable periodic solution of the constant forcing case is created.

Figures 10 and 11 plot various phase space slices of the orbits of the stable cases detailed in the above figures in hopes of gaining some insight into the dynamics.

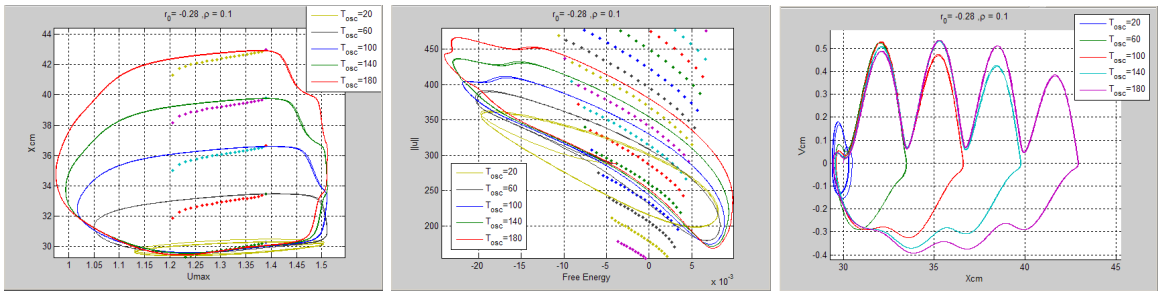

FIG. 10: Various phase space slices of solutions along $r_0 = -.28$ with $\rho = -0.1$ that are periodic in time. (a)The maximum height of the solution vs the position of the front. the motivation here was to graph the length and heigth of the solution to give some sense of its size. (b) The free energy of the solution vs the L2 norm. (c) the phase space of the front, the postion of the front vs its speed.

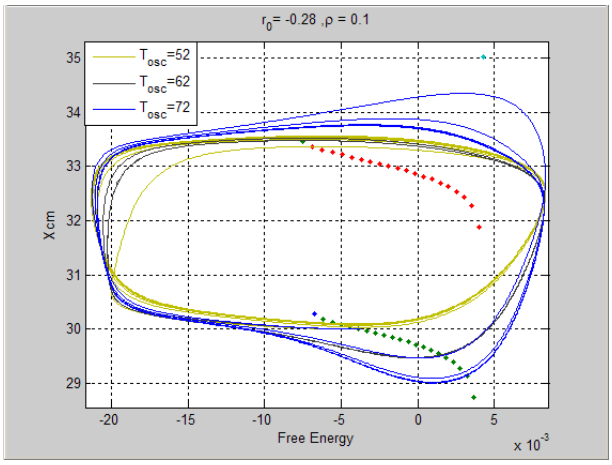

FIG. 11: Trajectories in phase space of an orbit at the edges and center of the stable region in parameter space.

IV. EFFECT OF SMALL OSCILLATIONS ON THE FRONT SPEED NEAR THE EDGE OF THE PINNING REGION

A. graph of numerical results - we don't really have this yet

B. asymptotic calculation and comparison to numerical result

Following Burke's calculation for the standard SHE to find the time between nucleation events, we derive an equation that estimates the effects of small, slow oscillations on the depinning process. We will perform this calculation just to the right of r_+, the right edge of the pinning region of the constant forcing case (e.g. $r \to r_+ + \epsilon^2\delta$). Note that the exact same procedure could be used to find the time between decay events just to the left of the pinning region. We will assume small (e.g. $\rho \to \epsilon^2\rho$), slow oscillations (e.g. $\omega \to \epsilon\omega$) so that the deviation from Burke's calculation will be small in this case. The equation, in this limit becomes

$$u_t = \left(r_+ + \epsilon^2(\delta + \rho \sin \epsilon\omega t)\right) u - \left(1 + \partial_x^2\right)^2 u + bu^2 - u^3, \tag{5}$$

where r_+ is the right edge of the pinning region when $\rho, \delta = 0$. Because we are near the pinning region, we can assume the dynamics will be slow and will define the slow timescale $\tau = \epsilon t$ and corresponding time derivative $\partial_t \to \epsilon\partial_\tau$. After writing u as an asymptotic series, $u = u_0 + \epsilon u_1 + \epsilon^2 u_2 + ...$, we can write out the equation order by order in ϵ. At leading order, we have

$$r_+ u_0 - \left(1 + \partial_x^2\right)^2 u_0 + bu_0^2 - u_0^3 = 0, \tag{6}$$

and can thus pick u_0 to be a localized solution at a saddle-node bifurcation of the snaking branch. Thus u_0 is stationary in time, but only marginally stable. Going on to order $\mathcal{O}(\epsilon)$, we get

$$\partial_\tau u_0 = r_+ u_1 - \left(1 + \partial_x^2\right)^2 u_1 + 2bu_0 u_1 - 3u_0^2 u_1 \tag{7}$$

Since we have chosen u_0 to be stationary in time, u_1 must be a zero eigenvector of the SHE linearized about the solution a the saddle-node of the snaking branch. Just as in Burke's calculation, the relevant eigenvector is the one that corresponding to the direction that adds periods to the localized solution (u_{amp}) and it conveniently has an eigenvalue of 0 since we are right on the saddle-node. Thus we can write the correction in the form $u_1 = a(\tau)u_{\text{amp}}$.

We must go on order $\mathcal{O}(\epsilon^2)$ to determine a. At this order, the equation is

$$\partial_\tau u_1 = r_+ u_2 - \left(1+\partial_x^2\right)^2 u_2 + 2bu_0u_2 - 3u_0^2u_2 + (\delta + \rho\sin\omega\tau)u_0 + bu_1^2 - 3u_0u_1^2 \tag{8}$$

Because the linear operator acting on u_2 is self-adjoint and u_{amp} is in it's nullspace, we use this equation to obtain the following solvability condition that determines a.

$$\alpha_1\dot{a} = \alpha_2(\delta + \rho\sin\omega\tau) + \alpha_3 a^2, \tag{9}$$

where

$$\begin{aligned}
\alpha_1 &= \int_0^L u_{\text{amp}}(x)^2 dx \\
\alpha_2 &= \int_0^L u_{\text{amp}}(x)u_0(x)dx \\
\alpha_3 &= \int_0^L u_{\text{amp}}(x)^3(b-3u_0(x))dx
\end{aligned} \tag{10}$$

Forour choice of parameters ($b = 1.8$) and a choice of normalization that sets $\alpha_1 = 1$, we find that $\alpha_2 \approx 0.9756$ and $\alpha_3 = 0.2863$ (from J. Burke thesis, need to calculate myself).

Under the proper rescaling of parameters (NEED TO BE CAREFUL ABOUT SIGNS OF COEFFICIENTS), the equation becomes

$$\dot{a} = 1 + \rho\sin\omega\tau \pm a^2. \tag{11}$$

Explicitly, we take:

$$\begin{aligned}
a &\to \sqrt{\frac{\alpha_3}{\delta\alpha_2}}a \\
\tau &\to \sqrt{\frac{\delta\alpha_2\alpha_3}{\alpha_1}}\tau \\
\rho &\to \frac{\rho}{\delta} \\
\omega &\to \frac{\alpha_1}{\sqrt{\delta\alpha_2\alpha_3}}\omega
\end{aligned} \tag{12}$$

in order to achieve the scaled equation. Here the sign is chosen by the sign of the product of $\alpha_2\alpha_3$. We also note that the scaled ρ will be less than one if the oscillation remains exclusively outside of the pinning region. Finally, we note that we can choose to normalize

u_{amp} such that $\alpha_1 = 1$. We can now make the transformation $a = \mp\dot{b}/b$ to put the equation into the form of a Mathiew equation:

$$\ddot{b} \pm (1 + \rho \sin \omega\tau)b = 0 \tag{13}$$

I ASSUME THE CALCULATION IS TAKEN TO THE RIGHT OF THE PINNING REGION. THE OTHER SIDE IS ANALOGOUS, BUT SHOULD I REWRITE THE FORMULAS SO THAT THEY DESCRIBE BOTH CASES? IT MAY MAKE THE WRITING A LITTLE MROE CONFUSING, BUT WOULD BE MORE GENERAL.

NEED TO ADD A DISCUSSION ABOUT THE INVERTED PENDULUM PROBLEM HERE.

V. STABILITY, GROWTH, AND DECAY OF LOCALIZED SOLUTIONS UNDER LARGE OSCILLATIONS

We now turn to oscillations of the forcing with an amplitude greater than that of the pinning region. The system, initialized with a localized solution that is stable for the constant forcing case at the center of the oscillation, will spend its time alternating between growth and decay. When the growth exactly balances the decay over the course of an oscillation, periodic solutions are produced that "breathe" with the oscillation period. Otherwise, we see either growth or decay of the localized solution that was once stable in the constant forcing case.

In many cases we consider, the oscillation even takes the system to beyond r_{SN} where there no longer exists a periodic solution. It is near this value of r that localized solutions in the constantly forced system decay by an overall amplitude decrease instead of by having periods decay symmetrically off of the ends. If the solution spends enough time in this region, the solution will decay to the trivial one no amount of time in in the region of growth will allow for recovery of the solution. Note that we have assumed that the system never leaves the region of stability for the trivial state (e.g. $r < 0$ for the entire oscillation).

A. Periodic oscillations of the solution

Given a particular oscillation amplitude, we find a range of values for the oscillation center (r_0) and oscillation period (T) that strikes the necessary balance between growth and

decay to create periodic solutions. For short periods where there is not enough time for nucleation and decay within an oscillation, the periodic solutions span the entire pinning region. While the general trend of the range is to narrow for increasing oscillation periods, it does not narrow monotically – "sweet spots" where the range is larger than the pinched regions above and below occur at regular intervals of the oscillation period. For $\rho = 0.1$ shown in Fig. 12, the region of existence of periodic orbits shifts to increased values of r_0. It asymptotes to near $r_0 \approx -.275$, which is just at the threshold when the system starts to spend time in the region where amplitude decay takes over period decay as the leading mode of decay. In the limit that the period goes to infinity, it is impossible to have a periodic orbit if the system spends any time in this region.

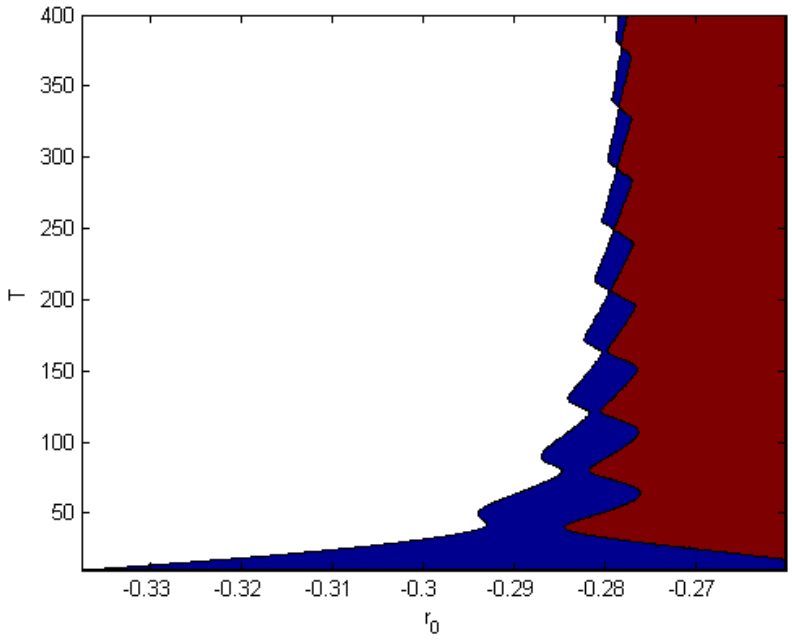

FIG. 12: Region of existence for periodic orbits with an amplitude of oscillation $\rho = 0.1$. The simulations is initialized with a localized solution that is stable with a constant forcing of r_0 and the blue region indicates where the solution does not grow or decay on average. The average velocity of the front is negative (e.g. the decaying) in the white region and positive (e.g. the solution is growing) in the red region.

Except for at very fast oscillations, the Maxwell point of the constant forced system falls to the left of the region of existence for periodic orbits. One might expect the orbits to be transients that are weakly unstable because they have a negative average energy and

leave the pinning region for an appreciable amount of time. However, Our simulations show (Fig. 13) that these periodic orbits persist for very long times and the change in the solution from one oscillation to the next exponentially decays to machine precision. The L_2 norm of the difference between the solutions at the start of each oscillation exponentially decay for three different sets of r_0 and T within the region of existence of periodic orbits. Space-time plots of the solution and phase space slices that show the front position and the maximum value of the solution are included for each of the converged orbits as well. The solution "breathes" more for longer period oscillations where the system spends longer timespans outside of the pinning region of the constant forcing case. Furthermore, there is an asymmetry between the rates of the growing and shrinking parts of the orbit because the nucleation process to the right of the pinning region happens slower than the decay process to the left.

We can also consider effect different amplitudes of the oscillation have on the stable region. Oscillations amplitudes must be greater than about $\rho \approx .04$ in order to exit both sides of the pinning region during one oscillation. As we increase the oscillation amplitude, the system spends a larger amount of time outside of the pinning region for a given oscillation period and a the system crosses the threshold into amplitude-dominated decay for a larger range of values of r_0. As a result, the pinching regions are stretched out in oscillation period T_{osc} and shifted to less negative values of r_0.

B. Growth and decay

For the solutions that do not form periodic orbits, we can classify their growth and decay in terms of the number of periods gained or lost after one full period of the forcing. This reveals a partition of the pinning region with a very regular structure (Fig. 15). In the upper left corner of the figure, there is a cliff that indicates where a localized solution that is stable with a constant forcing of r_0 will decay to zero within one oscillation via the amplitude decay. As we move the right, the different colored regions indicate the number of periods that are gained or lost after one full oscillation. The central region corresponds to the stable region of Fig. 12. Each successive band has an increase of one period per side growth (to the right) or decay (to the left) from the previous one. Striking are the upward and downward slanting curves that connect the edges of these regions (Fig. **??**). The downward slanting

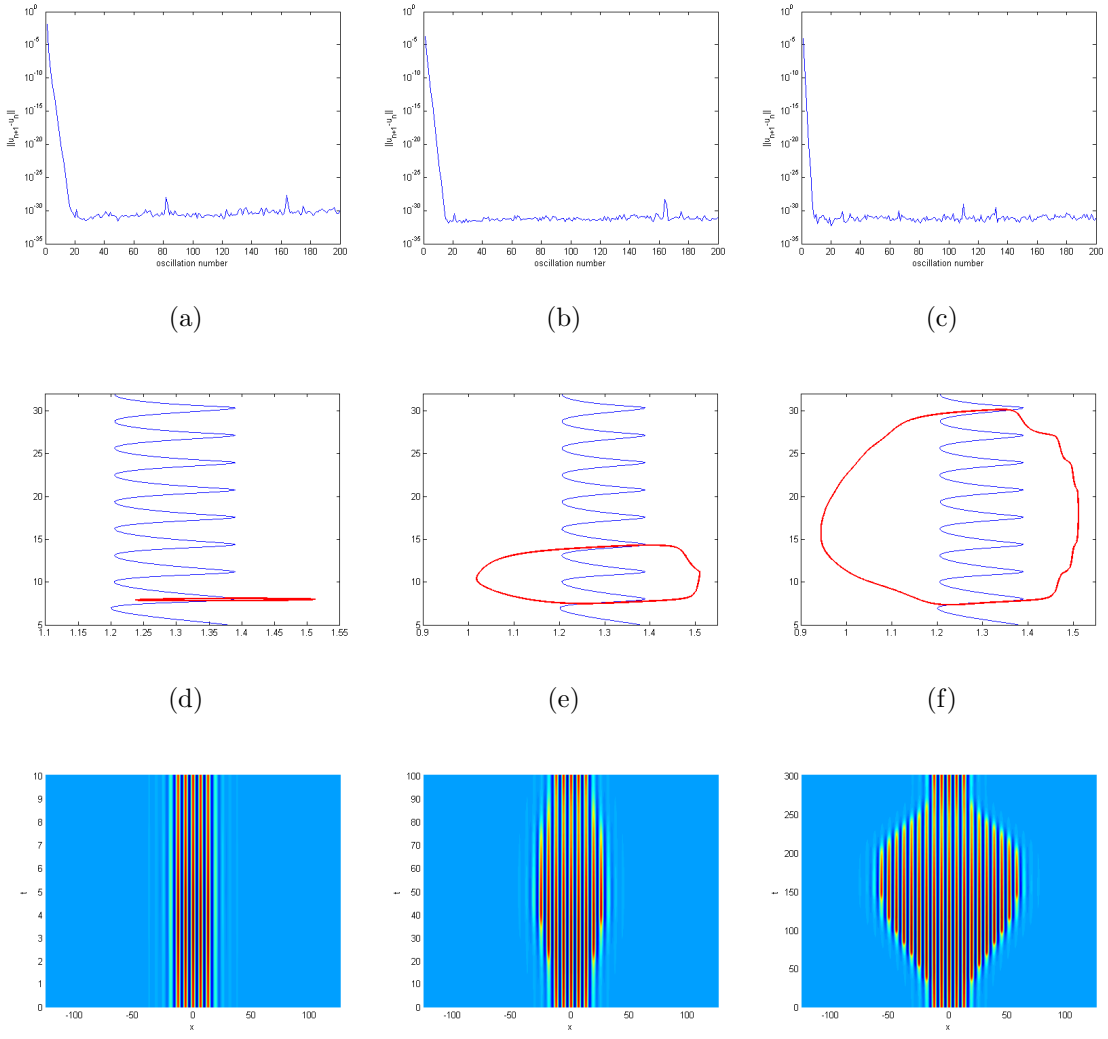

(a) (b) (c)

(d) (e) (f)

(g) $T = 10$, $r_0 = -0.26$ (h) $T = 100$, $r_0 = -0.28$ (i) $T = 300$, $r_0 = -0.279$

FIG. 13: Convergence of periodic orbits. W. (a)-(c) show the L_2 norm of the difference of the solution from one exactly one oscillation period prior. (d)-(f) show the corresponding trajectories of the converged orbit along the slice of front postion vs. amplitude and (g)-(i) show spacetime plots of the solution along one orbit.

curves are associated with the growing portion of the oscillation and indicate transitions to the number of periods gained during this part. At the bottom of the graph, the oscillation is too fast for any nucleations to occur. The solution gains one period per side within the band directly above, two in the band above this, and so on. In the upper righthand corner, the solution gains 12 periods during the part of the oscillation that the system is to the right

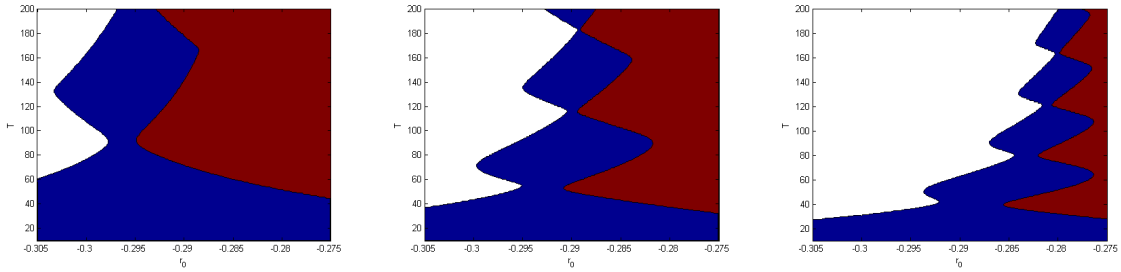

FIG. 14: The average speed at which the solution grows or decays as a function of oscillation period and oscillation center of the forcing parameter when (a)$\rho = 0.06$, (b)$\rho = 0.08$, (c)$\rho = 0.1$. The solution had decayed by one or more periods over the course of the simulation (20 oscillations of the forcing) in the white region, and has grown by one or more periods over the course of the simulation in the red region. The blue region indicates where the solution has not grown or decayed on average.

of the pinning region. A similar pattern occurs with the upward sloping curves, except that they are associated with the portion of the oscillation that takes the system to the left of the pinning region. The lines tend to accumulate at the cliff that marks the transition to amplitude-dominated decay. The boundaries between the regions are represented as lines here, but actually have a finite size. Figure 17 shows a horizontal slice of Fig. 15 at T=100. There are very clear plataues which correspond to an integer number of periods decaying in an oscillation, but there are also transition regions inbetween. A logarighmic plot of the size of the transition regions and plateues for decaying solution point to an accumulation point of these regions at the cliff. (SHOULD I INVESTIGATE THE GROWING SOLUTION PLATEAUS AND TRANSITIONS?) (NEED TO EXTRAPOLATE THE PLATEAU SIZES ON GRAPH)

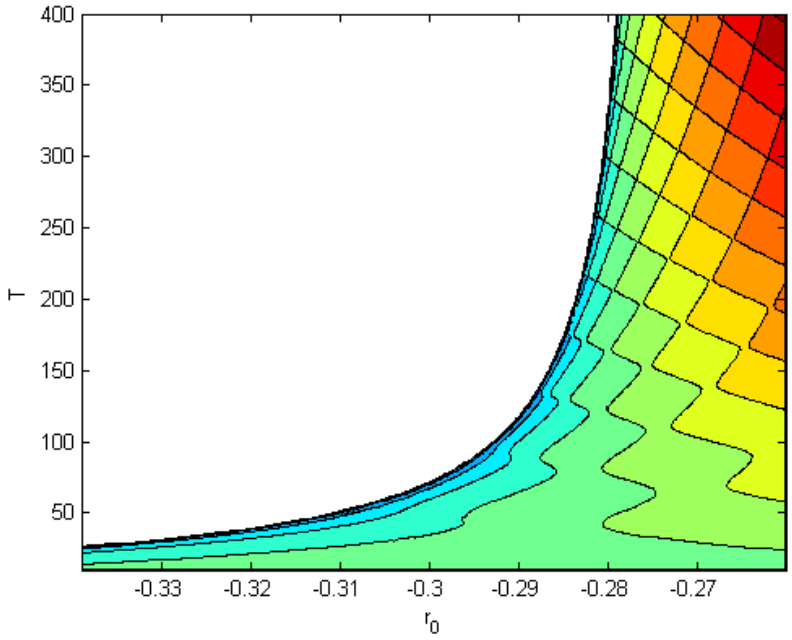

FIG. 15: Growth and decay of localized solutions with an amplitude of oscillation $\rho = 0.1$. The simulations is initialized with a localized solution that is stable with a constant forcing of r_0 and the central green region indicates where the solution does not grow or decay on average (corresponding to the blue region of Fig. **??**). The light blue region imediately to the left indicates decay by one period on each side per oscillation, the next one decays by two periods per oscillation, and so on. The solution grows by one period on each side per oscillation in the region immediately to the right, and this increases in integer values until 9 periods on a side per oscillation is reached in the upper right corner. The white region to the left indicates where amplitude decay dominates and the solution decays to the trivial one within one oscllation.

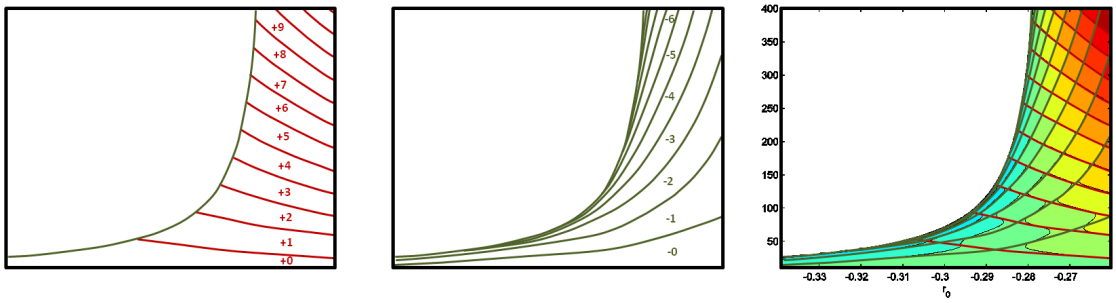

FIG. 16: Lines indicating transitions between the number of periods of (a) growth and (b) decay on each side of the localized solution during one oscillation of the forcing. There is a successive increase in the rate of growth and decay as one moves up the graph. The lines are superimposed over the data from numerical simulations in (c). The region of periodic solutions are where the growth matches the decay.

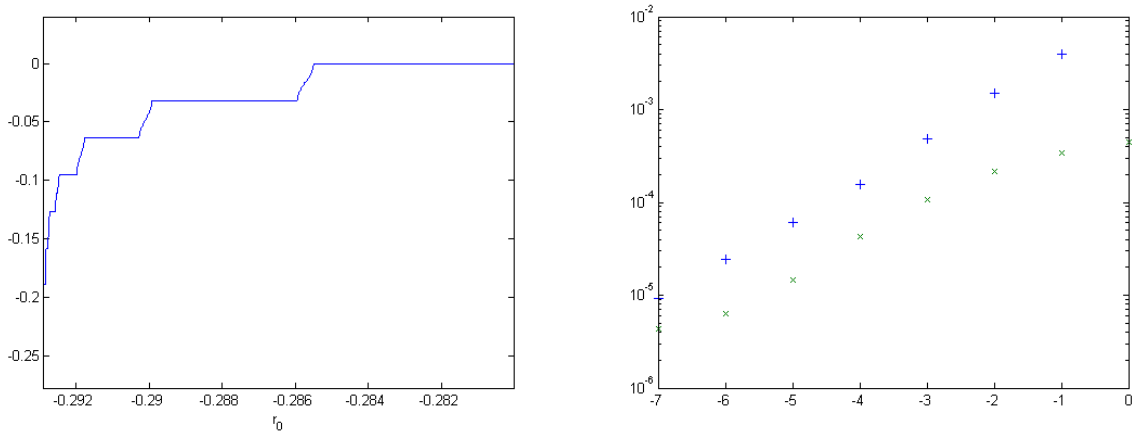

FIG. 17: (a) The speed of the front as a function of oscillation center r_0 with a fixed oscillation period $T = 100$ within the region of decay. The plateaus correspond to an integer number of period decays per oscillation. There is a cliff to the left marking the transition to amplitude-dominated decay as opposed to decay by front motion. (b) A logarithmic plot of the length of the plateau and the transition region, showing the approach of an accumulation point where the cliff forms.

1. stability lines and avoided crossings?

C. simple model interpretaion??

D. some asymptotic calculations???

VI. PERSISTENCE OF DEFECTS DUE TO OSCILLATIONS

Using an oscillation with a period of 50 and centered about $r_0 = -0.27$ and amplitude of $\rho = 0.1$, we can see the trajectory taken by the initial localized solution as it approaches a domain filling one (Fig. 18). The solution grows by nucleating a period on each front at each oscillation of the forcing parameter. This happens until the solution reaches 39 periods, at which point it seems to get stuck. Eventually it fills the domain with a 40 period solution. This is in contrast to the case with a constant forcing that grows into the domain with a 39 period solution.

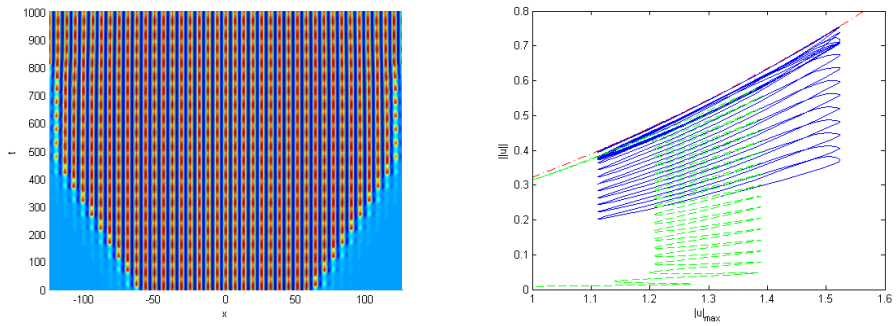

(a) (b)

FIG. 18: Oscillations of the forcing parameter in and out of the snaking region. The forcing parameter as a function of time is given by $r \to -0.27 + 0.1 \sin 2\pi t/50$. The solution (a) grows in time, eventually filling the domain and the corresponding trajectory along the max value - L2 norm phase space slice (b) shows the path taken as it passes in and out of the snaking region .

A. show solutions of quasistable defect connecting to both 39 and 40 period solution as well as stable defect

B. graph of regions where for each case

C. Some kind of explanaition (Eckaus instability and delayed bifurcations?)

VII. CONCLUSION

A. summarize results

B. future directions

---

[1] Assaf Y Kletter, Jost von Hardenberg, and Ehud Meron, "Ostwald ripening in dryland vegetation," Comm Pure Appl Anal **11**, 261–273 (2012).

[2] Mustapha Tlidi, René Lefever, and A Vladimirov, "On vegetation clustering, localized bare soil spots and fairy circles," in *Dissipative Solitons: From Optics to Biology and Medicine* (Springer, 2008) pp. 1–22.

[3] Ehud Meron, "Pattern-formation approach to modelling spatially extended ecosystems," Ecological Modelling **234**, 70–82 (2012).

[4] Jonathan A Sherratt, "Pattern solutions of the klausmeier model for banded vegetation in semi-arid environments i," Nonlinearity **23**, 2657 (2010).

[5] Jonathan A Sherratt, "An analysis of vegetation stripe formation in semi-arid landscapes," Journal of mathematical biology **51**, 183–197 (2005).

[6] Igor Belykh, Vladimir Belykh, Russell Jeter, and Martin Hasler, "Multistable randomly switching oscillators: The odds of meeting a ghost," The European Physical Journal Special Topics **222**, 2497–2507 (2013).

[7] J Buceta, Katja Lindenberg, and JMR Parrondo, "Stationary and oscillatory spatial patterns induced by global periodic switching," Physical review letters **88**, 024103 (2001).

[8] J Swift and Pierre C Hohenberg, "Hydrodynamic fluctuations at the convective instability," Physical Review A **15**, 319 (1977).

[9] John Burke and Edgar Knobloch, "Localized states in the generalized swift-hohenberg equation," Physical Review E **73**, 056211 (2006).

[10] John Burke and Edgar Knobloch, "Snakes and ladders: localized states in the swift–hohenberg equation," Physics Letters A **360**, 681–688 (2007).

[11] John Burke and Edgar Knobloch, "Homoclinic snaking: structure and stability," Chaos: An Interdisciplinary Journal of Nonlinear Science **17**, 037102–037102 (2007).

[12] SM Cox and PC Matthews, "Exponential time differencing for stiff systems," Journal of Computational Physics **176**, 430–455 (2002).

[13] Eusebius J Doedel, "Auto: A program for the automatic bifurcation analysis of autonomous systems," Congr. Numer **30**, 265–284 (1981).

[14] Alain Bergeon, J Burke, E Knobloch, and I Mercader, "Eckhaus instability and homoclinic snaking," Physical Review E **78**, 046201 (2008).

[15] José MG Vilar and JM Rubi, "Spatiotemporal stochastic resonance in the swift-hohenberg equation," arXiv preprint cond-mat/9702205 (1997).

[16] A. M. Rucklidge and M. Silber, "Design of parametrically forced patterns and quasipatterns," SIAM J. Appl. Math. **8**, 298–347 (2009).

[17] O. Batiste, E. Knobloch, A. Alonso, and I. Mercader, "Spatially localized binary-fluid convection," J. Fluid Mech. **560**, 149–158 (2006).

[18] T. M. Schneider, J. Gibson, and J. Burke, "Snakes and ladders: localized solutions of plane Couette flow," Phys. Rev. Lett. **104**, 104501 (2010).

[19] C. Beaume, H.-C. Kao, E. Knobloch, and A. Bergeon, "Localized rotating convection with no-slip boundary conditions," Phys. Fluids **25**, 124105 (2013).

[20] C. Beaume, A. Bergeon, and E. Knobloch, "Convectons and secondary snaking in three-dimensional natural doubly diffusive convection," Phys. Fluids **25**, 024105 (2013).